

# Superior low-cycle fatigue properties of CoCrNi compared to CoCrFeMnNi

Kaiju Lu<sup>1\*</sup>, Ankur Chauhan<sup>1\*\*</sup>, Mario Walter<sup>1</sup>, Aditya Srinivasan Tirunilai<sup>2</sup>, Mike Schneider<sup>3</sup>, Guillaume Laplanche<sup>3</sup>, Jens Freudenberger<sup>4,5</sup>, Alexander Kauffmann<sup>2</sup>, Martin Heilmaier<sup>2</sup>, and Jarir Aktaa<sup>1</sup>

email: [\\*kaiju.lu@kit.edu](mailto:kaiju.lu@kit.edu); [\\*\\*ankurskchauhan@gmail.com](mailto:ankurskchauhan@gmail.com)

<sup>1</sup>Institute for Applied Materials, Karlsruhe Institute of Technology (KIT), Hermann-von-Helmholtz-Platz 1, 76344 Eggenstein Leopoldshafen, Germany

<sup>2</sup>Institute for Applied Materials, Karlsruhe Institute of Technology (KIT), Engelbert-Arnold-Strasse 4, 76131 Karlsruhe, Germany

<sup>3</sup>Institut für Werkstoffe, Ruhr-Universität Bochum, D-44801, Bochum, Germany

<sup>4</sup>Leibniz Institute for Solid State and Materials Research Dresden (IFW Dresden), Helmholtzstr. 20, D-01069 Dresden, Germany

<sup>5</sup>Institute of Materials Science, Technische Universität Bergakademie Freiberg, Gustav-Zeuner-Str. 5, 09599 Freiberg, Germany

## Abstract

We report on the low-cycle fatigue behavior of single-phase, face-centered cubic CoCrNi and CoCrFeMnNi at room temperature. Both alloys manifest cyclic hardening followed by softening and a near steady state until failure. CoCrNi exhibits higher strength, lower inelastic-strain, and longer lifetime than CoCrFeMnNi. For both alloys, microstructural investigations reveal no noticeable changes of texture, grain size and twin fraction. Nevertheless, CoCrNi exhibits planar dislocation structures, while CoCrFeMnNi shows well-defined wavy dislocation structures. This is due to CoCrNi lower stacking fault energy, which enhances planar slip and delays deformation localization leading to its superior fatigue resistance, compared to CoCrFeMnNi.

**Keywords:** High- and medium-entropy alloys; Fatigue; Transmission electron microscopy (TEM); Dislocation structure.

High-entropy alloys (HEAs) that consist of multiple principal elements and form concentrated solid solutions, have gained huge scientific interest [1-3]. Among them, CoCrFeMnNi with face-centered cubic (FCC) crystal structure has attracted significant attention for its exceptional combination of mechanical properties [4-9], *e. g.*, at 77 K and for a mean grain size of  $\sim 6 \mu\text{m}$ , CoCrFeMnNi has a tensile strength of  $\sim 1.2 \text{ GPa}$ , an elongation to failure of  $\sim 70\%$ , and fracture toughness of  $\sim 220 \text{ MPa}\sqrt{\text{m}}$  [4, 5]. Other studies revealed that a subset of equiatomic alloys from the Co-Cr-Fe-Mn-Ni system, most notably the FCC CoCrNi medium-entropy alloy (MEA) exhibits an even better combination of mechanical properties [4-9], *e. g.*, an ultimate tensile strength of  $\sim 1.3 \text{ GPa}$ , an elongation to failure of  $\sim 90\%$  and a fracture toughness of  $\sim 270 \text{ MPa}\sqrt{\text{m}}$  at 77 K for a non-uniform grain size of 5-50  $\mu\text{m}$  [10]. The main reasons for the superior mechanical properties of CoCrNi are (1) its higher shear modulus and (2) an earlier onset of deformation twinning due to its lower ( $\sim 25\%$ ) stacking fault energy (SFE) compared to CoCrFeMnNi [8, 11, 12]. The formation of numerous nanotwins impedes dislocation motion and leads to an enhanced work-hardening, which delays the onset of necking; hence, resulting in enhanced strength and ductility. To date, comprehensive studies have shed light mostly on the monotonic deformation behavior of CoCrNi and related alloys [4-9, 13]. However, engineering alloys are usually not only loaded monotonically in service but also cyclically. Few studies, concerning the fatigue properties of HEAs have been reported [14-19], where it was shown that CoCrFeMnNi demonstrates a higher low-cycle fatigue (LCF) resistance compared to common FCC steels [14, 19]. Recently, Rackwitz et al. [20] revealed a superior fatigue crack propagation resistance of CoCrNi compared to CoCrFeMnNi [21], especially at cryogenic temperatures, where the increased propensity of nanotwinning decreased the crack growth rate. However, to our knowledge, investigations concerning the LCF behavior of CoCrNi have not yet been reported.

Considering the superior mechanical properties of CoCrNi compared to CoCrFeMnNi, it could be anticipated that CoCrNi would exhibit a better LCF resistance. It is known that the fatigue behavior of FCC materials is strongly associated with their dislocation slip mode, *i.e.*, planar slip or cross/wavy slip [22]. Some prominent dislocation structures include persistent slip bands (PSBs), cells and/or veins structures, as well as planar slip bands (SBs) and stacking faults (SFs). The formation of the two former dislocation structures are widely reported in FCC materials with high SFEs [23-29]. Among them, PSBs typically comprise full (non-dissociated) edge dislocations with the same Burgers vector that usually form in single-slip oriented grains [23-27]. Veins or cells-like structures are known to form due to cross-slip of full screw dislocations [28, 29]; thus, indicating activation of secondary slip systems [22, 27]. In contrast, planar SBs, and SFs are typical dislocation structures in materials with low SFEs [29-31]. With

CoCrNi and CoCrFeMnNi, there are two alloys from the family of medium- and high-entropy alloys that differ in their SFE, while that of CoCrNi is lower. Hence, the present study is designed to identify the LCF behavior and the related microstructural evolution of both alloys and to identify if the observed difference is driven by the SFE.

The investigated CoCrNi and CoCrFeMnNi alloys were synthesized from pure metals (with at least 99.9 wt% purity) by vacuum induction and arc melting, respectively. The CoCrNi melt was poured in a cylindrical steel mold with a 45 mm diameter that was coated with a zirconia slurry while the CoCrFeMnNi melt was drop cast in a cylindrical water-cooled copper mold with diameter of 14 mm. The as-cast ingots were homogenized at 1473 K for 48 h and 72 h and water-quenched. Subsequently the alloys were rotary swaged to ~6 mm in diameter with an areal reduction per pass of  $\epsilon \approx 0.19$ . LCF specimens with a gauge length of 7.6 mm and a gauge diameter of 2 mm were machined out from the rotary-swaged rods. Finally, to obtain single-phase FCC alloys with a recrystallized microstructure as well as a comparable grain size, LCF specimens were annealed for 1 h at 1098 K for CoCrNi and at 1073 K for CoCrFeMnNi. More details about the processing of CoCrNi and CoCrFeMnNi can be found in Refs. [8, 32].

LCF tests were performed on an MTS servo-hydraulic testing machine equipped with an extensometer of 7 mm in gauge length. The strain-controlled tests were carried out at room temperature (RT) using total strain amplitudes of 0.3%, 0.5%, 0.6%, and 0.7%. A symmetrical triangular waveform ( $R = -1$ ) was employed at a nominal strain rate of  $3 \times 10^{-3} \text{ s}^{-1}$ . For given testing parameters, at least two experiments were carried out to evaluate the reliability of the data.

To reveal the microstructural evolution, initial and deformed microstructures were characterized *via* electron backscatter diffraction (EBSD) and transmission electron microscopy (TEM). For EBSD, an FEI Nova scanning electron microscope equipped with an HKL detector was employed at an accelerating voltage of 20 kV and a step size of 200 nm. Thin strips from the gauge section of the tested samples were extracted out parallel to the loading direction. These strips were then mechanically ground and polished. The acquired EBSD data were analyzed using the OIM analysis software. In order to prepare TEM samples, the strips were further mechanically ground to a thickness of ~100  $\mu\text{m}$ . Thereafter, the foils were thinned down to electron transparency by electro-polishing using a Struers TenuPol-5 device at -20 °C and a voltage of 13 V. The electrolyte consisted of 10% perchloric acid, 20% glycerin, and 70% methanol. TEM investigations were performed on an FEI Tecnai F20 microscope operating at 200 kV.

The tensile peak stress and inelastic strain amplitude are presented in Fig. 1a-b, respectively, as a function of the normalized number of cycles ( $N/N_f$ ), for CoCrNi and CoCrFeMnNi at different strain amplitudes. Similar curves showing these evolutions with the number of cycles can be found in the supplementary material (Fig. S1a-b). The cyclic stress (i.e., tensile peak stresses) response of both materials in Fig. 1a can be divided into three stages: an increase (cyclic hardening stage), followed by a significant decrease (cyclic softening stage), and finally by a minor change (near steady state) until failure. While the initial cyclic hardening stage takes place during the first 20 to 30 cycles, the following cyclic softening stage represents ~10% of the lifetime for CoCrNi and 2% for CoCrFeMnNi. This indicates that for both alloys the significant changes in the cyclic stress response represent only small fractions of the lifetime. In other words, the majority of the lifetime is spent in a near steady state. The inelastic strain response in Fig. 1b is consistent with the evolution of the peak stress, i.e., it mainly manifests an initial sharp decrease followed by a gradual increase and near steady state until failure.

CoCrNi exhibits higher cyclic strength and lower inelastic strain than CoCrFeMnNi for all tested strain amplitudes (Fig. 1 and Fig. S1). The lower inelastic strain amplitude in CoCrNi is related to its higher elastic strain due to its higher cyclic/yield strength despite the higher elastic modulus, see Fig. S2. Higher yield strength of CoCrNi has been reported several times, see Refs [6-8], and originates from two distinct contributions: (1) higher solid solution strengthening [33, 34] and (2) larger grain boundary strengthening [5, 35], with the latter showing a stronger magnitude (3 to 5 times larger than the former) for a fine grain size of ~7  $\mu\text{m}$ .

Fig. 1c and d present the double-logarithmic plot of the stress amplitude ( $\Delta\sigma/2$ ) versus number of cycles to failure ( $N_f$ ) (i.e., S-N curve) and the inelastic strain amplitude ( $\Delta\varepsilon_{in}/2$ ) versus number of reversals to failure ( $2N_f$ ), curves, respectively. The  $\Delta\sigma/2$  and  $\Delta\varepsilon_{in}/2$  values were determined from the hysteresis loops at half-life ( $N_f/2$ ), where  $\Delta\varepsilon_{in}/2$  is the half-width of the hysteresis loops at zero stress. For a given stress amplitude (Fig. 1c) or inelastic strain amplitude (Fig. 1d), CoCrNi exhibits a longer fatigue life than CoCrFeMnNi. The data of each alloy in Fig. 1d follow the well-known power-type relationship (i.e., Coffin-Manson law,  $\Delta\varepsilon_{in}/2 = \varepsilon'_f (2N_f)^c$ ) [36, 37]. The fitted plots, functions and parameters are presented in Fig. 1d. The values of parameter  $c$  for both alloys are within the typical range ( $-0.7 \leq c \leq -0.5$ ) observed for most metals [29]. CoCrNi exhibits a lower  $c$  value, consistent with its longer LCF lifetime than CoCrFeMnNi [38]. Since the parameter  $\varepsilon'_f$  is related to the monotonic test's fracture strain [29, 36, 37], the obtained  $\varepsilon'_f$  for CoCrNi is, as expected, larger than that of CoCrFeMnNi. This evidence suggests that the

other medium-entropy subsystems of the CoCrFeMnNi with smaller fracture strains [6] may exhibit lower LCF resistance.

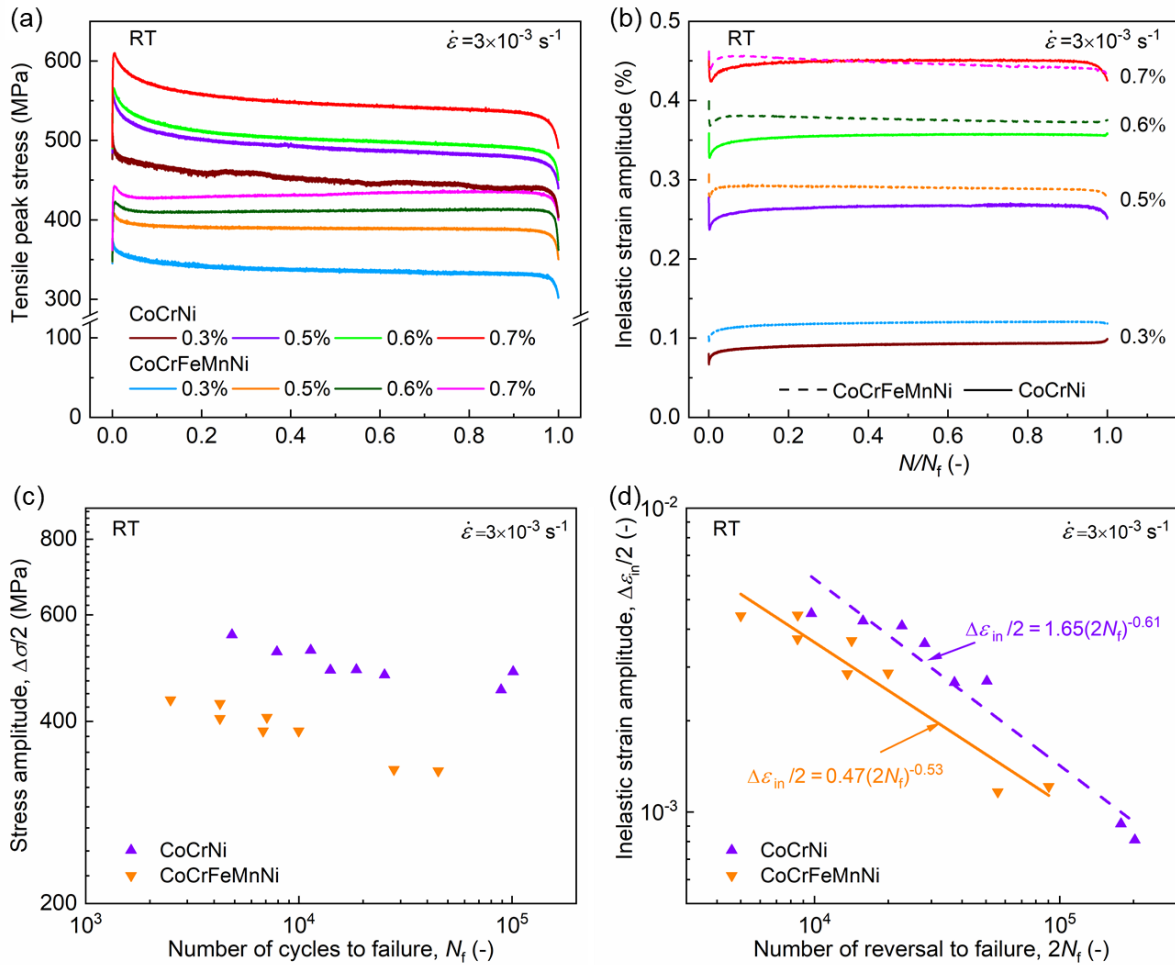


Fig. 1. (a) Tensile peak stress and (b) inelastic strain amplitude *versus* normalized number of cycles ( $N/N_f$ ), curves at different strain amplitudes, (c) stress amplitude ( $\Delta\sigma/2$ ) *versus* number of cycles to failure ( $N_f$ ), (d) inelastic strain amplitude ( $\Delta\epsilon_{in}/2$ ) *versus* number of reversals to failure ( $2N_f$ ) of CoCrNi and CoCrFeMnNi under different strain amplitudes. The fitted curves, functions and parameters using the Coffin-Manson law are displayed in (d).

Fig. 2a-b display representative overlaid image quality (IQ) and inverse pole figure (IPF) maps of an as-recrystallized CoCrNi and CoCrFeMnNi acquired *via* EBSD perpendicular to the swaging direction. IPF maps confirm that both investigated alloys are single-phase with FCC structure. Both alloys exhibit a weak  $\langle 111 \rangle$  and  $\langle 100 \rangle$  texture, which is typical for recrystallized, rotary-swaged FCC alloys [8, 32]. Additionally, the alloys possess equiaxed grains, with an average grain size of  $\sim 6 \pm 3 \mu\text{m}$ , and a high density of annealing twins due to their low to medium SFEs

[8, 32]. The initial dislocation density is low in both investigated materials, as shown in the bright-field TEM micrographs in Fig. 2c-d.

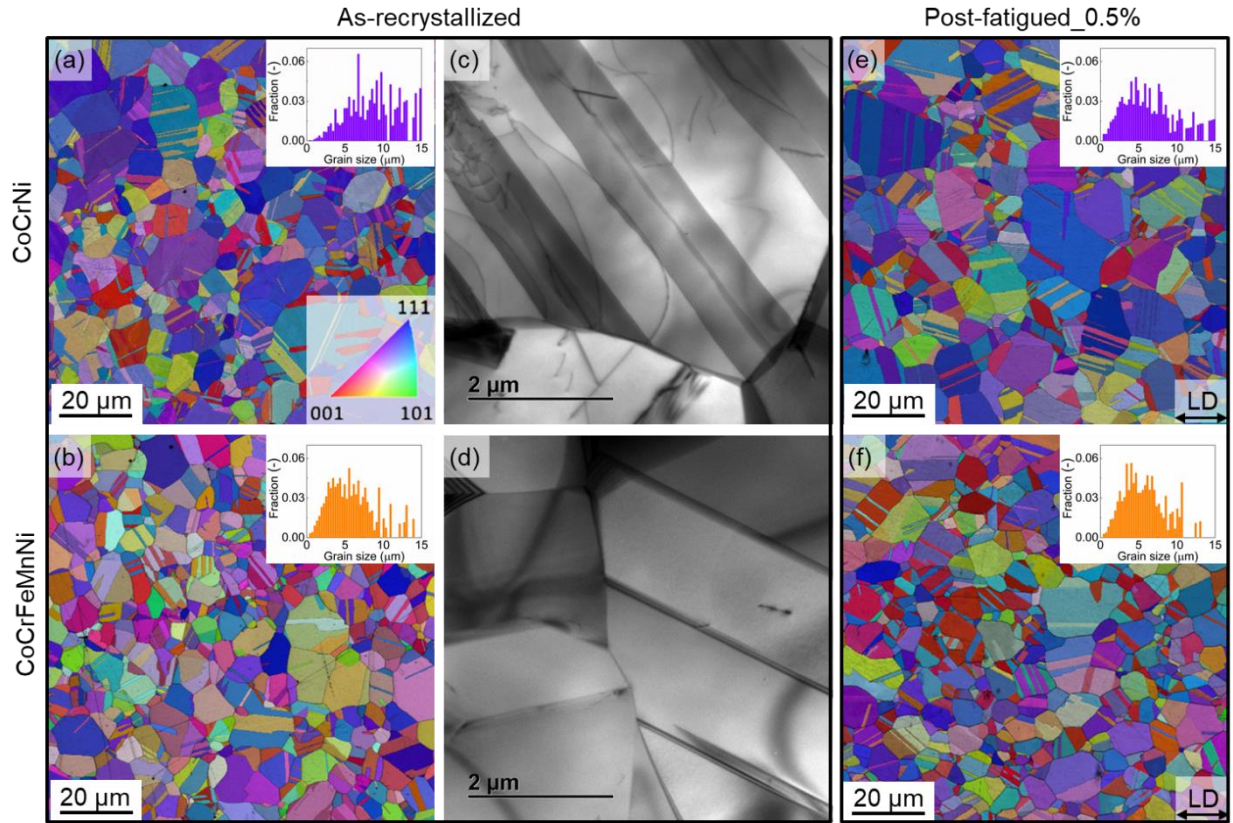


Fig. 2. Microstructures (a-d) in the recrystallized condition prior to fatigue testing and (e-f) in the post-fatigued (tested to failure at 0.5% strain amplitude) state of CoCrNi and CoCrFeMnNi: (a, b, e, f) overlaid image quality (IQ) and inverse pole figure (IPF) maps with color code plotted along the swaging direction. The grain size distributions of each states were provided in the inset of (a, b, e, f). (c, d) Bright-field TEM micrographs. Upon comparing IPF maps before and after deformation, both alloys exhibit no appreciable evolution of texture, grains size and annealing twins fraction.

Fig. 2e-f provide representative overlaid IQ and IPF maps of post-fatigued CoCrNi and CoCrFeMnNi, respectively, tested at an intermediate strain amplitude of 0.5%. Upon comparison with the as-recrystallized states (Fig. 2a-b), the IPF maps reveal no noticeable changes of texture, grain size and annealing twin densities after fatigue tests. However, detailed TEM investigations on both alloys reveal a high density of dislocations with distinct structures.

In post-fatigued CoCrNi, typical dislocation structures include stacking faults (SFs), slip bands (SBs), tangles and ill-defined dislocation walls or vein-like structures (see Fig. 3). Out of all, SFs and SBs, along with their debris, are the most prominent structures observed (see Fig. 3a-d). In

several grains, SFs and SBs are extended on different slip planes, *e.g.*, see marked A, B, C and D in Fig. 3a. When edge-on, SBs appear as straight parallel dislocation configurations, as shown in Fig. 3b. Besides, mostly individual dislocations present in a pile up (SB) are found to be dissociated into Shockley partials with a narrow SF in between (see Fig. 3c-d). Additionally, dislocations also appear to have interacted on multiple slip systems and formed tangled structures (see Fig. 3e). Finally, ill-organized dislocation vein-like structures were sporadically observed (see Fig. 3f).

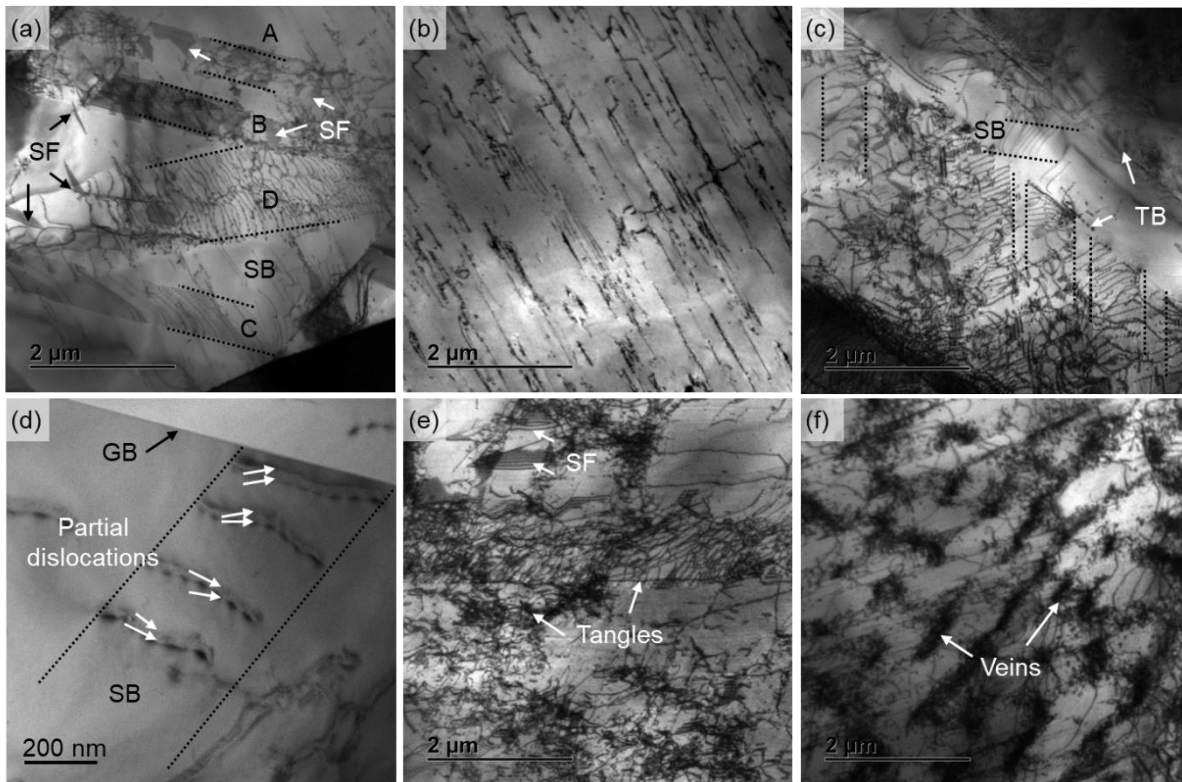


Fig. 3. Bright-field TEM micrographs of post-fatigued CoCrNi tested with a 0.5% strain amplitude at RT revealing typical dislocation structures, including (a-c) stacking faults (SFs) and slip bands (SBs). (b) Edge-on SBs appearing as straight parallel dislocation configurations. (c-d) Interactions of an SB with annealing twin boundary (TB) and grain boundary (GB). (d) Observed individual dislocations in SBs are dissociated into Shockley partials that are highlighted with pairs of arrows. (e) Dislocation tangles and SFs, and (f) Sporadically observed ill-organized dislocation walls or veins-like structures.

In ruptured CoCrFeMnNi, as evident in Fig. 4, mostly well-defined dislocation substructures (*i.e.*, dense walls of dislocations separated by low-dislocation density channels) were observed. Some dense walls tend to be parallel to each other (see regions A-E in Fig. 4). Others are also arranged in an irregular manner (see arrows in Fig. 4). These dislocation substructures are known to be veins and/or cells-like structures. Careful observations in both materials revealed no

deformation twinning, as seen under monotonic tensile tests [8, 39]. This observation is consistent with the fact that the critical stress required for the onset of twinning has not been reached in both alloys during cyclic loading. Indeed, for CoCrNi and CoCrFeMnNi, the critical twinning stresses were reported to be  $(740 \pm 45)$  MPa [8] and  $(720 \pm 30)$  MPa [39] respectively, for similar grain sizes.

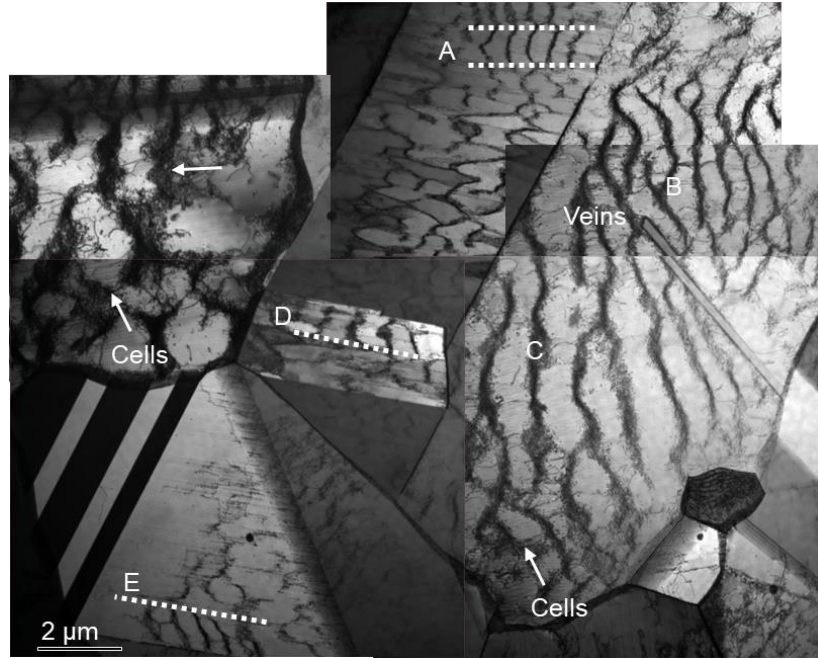


Fig. 4. Stitched bright-field TEM micrographs showing a representative post-fatigued microstructure of the CoCrFeMnNi tested with a strain amplitude of 0.5% at RT. Well-defined dislocation substructures, such as veins (marked A-E) and cells (indicated by arrows) suggest the domination of wavy slip behavior.

The cyclic stress response of materials is related to the associated microstructural evolution. Initially, grain-to-grain misorientations including plastic strain incompatibilities between grains, result in a significant increase in dislocation density close to the grain boundaries. Upon further cycling, as dislocations multiply and spread across grains, they interact (including activity of secondary slip) leading to cyclic hardening [14]. For CoCrNi, additional interactions between dislocations and SFs as well as SBs (that form concurrently) also contribute to the cyclic hardening. Once interior dislocations become abundant and occupy a much larger portion of the grains than boundaries, they start to annihilate and simultaneously rearrange into stable low-energy configurations (e.g., veins and/or cells [22, 40]) with high/low dislocation-density regions. This leads to a net reduction of the dislocation density, resulting in cyclic softening. Finally, as dislocation multiplication and annihilation reach an equilibrium, no significant change in dislocation densities and their structures lead to a quasi-stable cyclic response (near steady

state) until failure [14]. Moreover, the local-chemical short-range ordering (SRO) has been reported to exist in aged CoCrNi [41]. During deformation, SRO in aged CoCrNi has been linked to both hardening (as dislocations shear SRO domains) and subsequent glide plane softening (as favorable dislocation paths are introduced) [41]. Though, we could not yet prove the presence or absence of SRO in the investigated alloys, if present, it could also contribute to the evolution of the cyclic stress response.

From the above-mentioned investigations, the distinct dislocation structures observed for two alloys provide an insight into the reason for the difference in their LCF resistance. It is evident that the localized low-energy dislocation structures (*i.e.*, veins and/or cells) are more dominantly observed in CoCrFeMnNi than in CoCrNi. This is due to CoCrFeMnNi comparatively higher SFE of  $(30 \pm 5)$  mJ/m<sup>2</sup> [12], which facilitates partial dislocations constriction into full dislocations and allows cross-slip. These localized dislocation structures are associated with the development of extrusions and intrusions on the specimens surface, where fatigue cracks are known to nucleate [25, 42]. In contrast, due to its relatively lower SFE of  $(22 \pm 4)$  mJ/m<sup>2</sup> [8], the constriction of partial dislocations in CoCrNi is retarded, which reduces the propensity of dislocation cross-slip and rearrangement [28]. Therefore, CoCrNi mainly manifests planar dislocation structures (*i.e.*, SBs and SFs) [29-31]. This delays deformation localization in CoCrNi, leading to its superior LCF resistance, in comparison to CoCrFeMnNi. It is noteworthy that, apart from SFEs, grain orientation, applied strain amplitude, and cycle number have been reported to influence the observed dislocation structures upon cycling [22, 40, 42-47]. For instance, Pham et al. [40, 47] and Nellesen et al. [46] reported increasing strain amplitude and/or cycle number accelerates the formation of more complex and dense substructures (such as veins) in the LCF response of austenitic stainless steels. Nellesen et al. [46] also addressed the evolution of dislocation patterns from individual dislocations, clustering and loose veins up to well-pronounced and condensed veins as a function of grain orientation. Further studies concerning the above-mentioned aspects in the investigated materials are undergoing and will be reported separately.

In summary, both CoCrNi and CoCrFeMnNi show similar cyclic stress response with initial hardening followed by softening and a near steady state until failure, which represents ~90% of the alloy lifetime. Additionally, in comparison to CoCrFeMnNi, CoCrNi exhibits higher cyclic strength, lower inelastic strain, and longer lifetime for the same testing condition. For both alloys, microstructural investigations reveal no evident evolution in texture, grains size and twin fraction. However, detailed TEM investigations of ruptured specimens tested at an intermediate applied strain amplitude of 0.5% reveal distinct deformation behaviors. In post-fatigued CoCrNi, apart

from sporadic ill-defined vein-like dislocations structures, strain accumulates uniformly, mainly in the form of planar dislocation structures (including SBs and SFs). In contrast, in post-fatigued CoCrFeMnNi, full-dislocations rearrange themselves leading to well-defined wavy dislocations structures (i.e. veins and/or cells-like structures), causing strain localization. Therefore, due to CoCrNi relatively lower SFE, enhanced planar slip delays deformation localization leading to its superior fatigue resistance, in comparison to CoCrFeMnNi.

## Acknowledgment

AK and AST gratefully acknowledge financial support by the Deutsche Forschungsgemeinschaft within the framework of the Priority Program “Compositionally Complex Alloys - High-Entropy Alloys (CCA-HEA)” (SPP 2006), grant no. KA 4631/1-1. GL and MS also acknowledge funding from the Deutsche Forschungsgemeinschaft through project B8 of the SFB/TR 103.

## Supplementary material

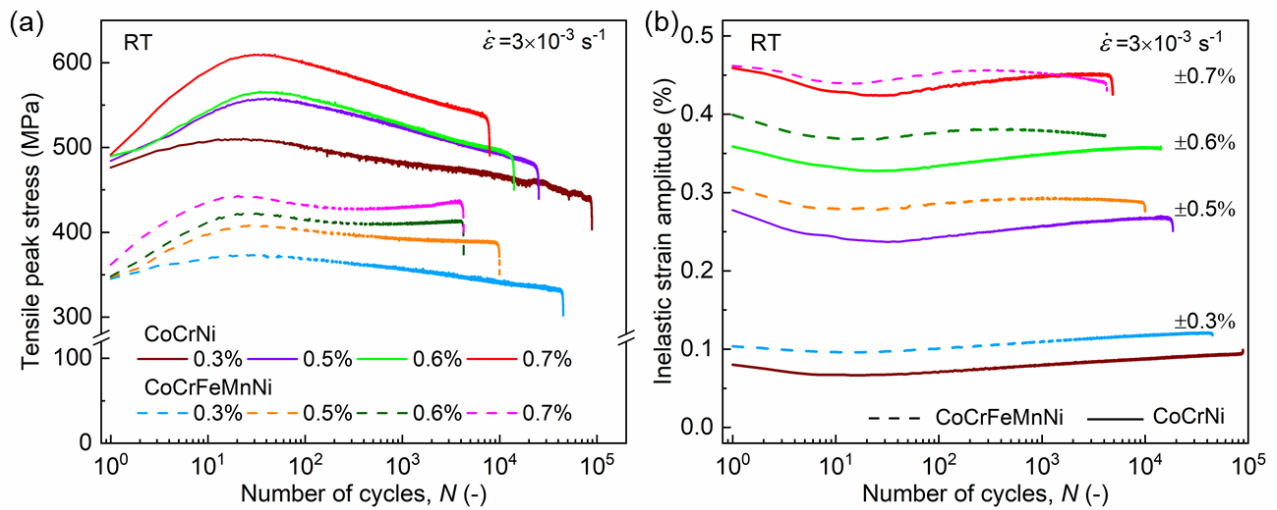


Fig. S1. (a) Tensile peak stress and (b) inelastic strain amplitude *versus* number of cycles ( $N$ ) curves for CoCrNi and CoCrFeMnNi under different strain amplitudes.

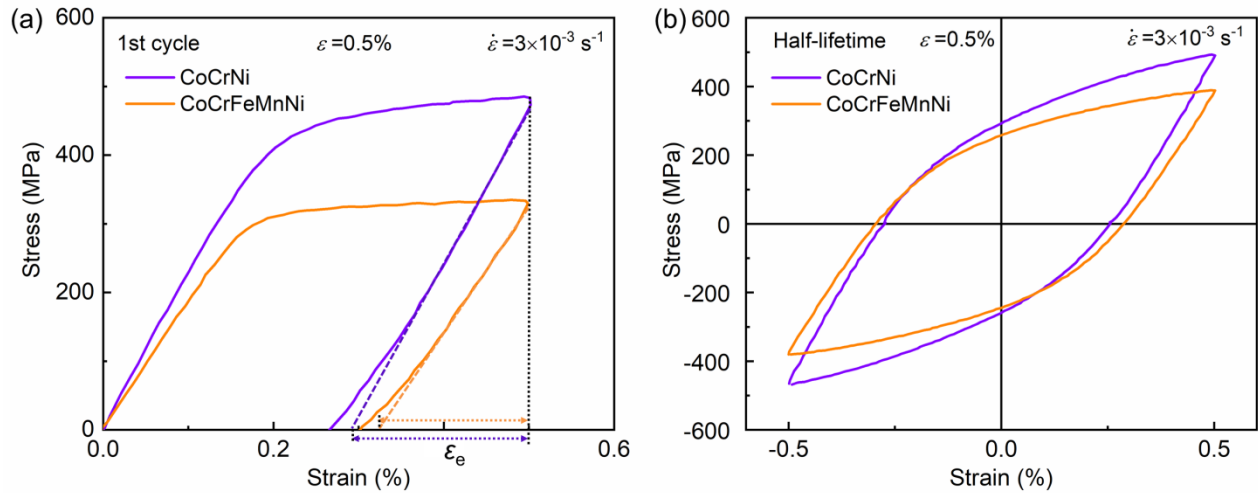


Fig. S2. (a) Stress-strain curves of the first quarter of the first cycle, and (b) half-life hysteresis loops for CoCrNi and CoCrFeMnNi tested at 0.5% strain amplitude at RT. Both figures show that CoCrNi exhibits higher cyclic strength and lower inelastic strain than CoCrFeMnNi.

## References

- [1] J.W. Yeh, S.K. Chen, S.J. Lin, J.Y. Gan, T.S. Chin, T.T. Shun, C.H. Tsau, S.Y. Chang, *Advanced Engineering Materials* 6(5) (2004) 299-303.
- [2] J.W. Yeh, Y.L. Chen, S.J. Lin, S.K. Chen, *High-entropy alloys—a new era of exploitation*, *Materials Science Forum*, Trans Tech Publ, 2007, pp. 1-9.
- [3] B. Cantor, I.T.H. Chang, P. Knight, A.J.B. Vincent, *Materials Science and Engineering: A* 375-377 (2004) 213-218.
- [4] B. Gludovatz, A. Hohenwarter, D. Catoor, E.H. Chang, E.P. George, R.O. Ritchie, *Science* 345 (6201) (2014) 1153-1158.
- [5] F. Otto, A. Dlouhý, C. Somsen, H. Bei, G. Eggeler, E.P. George, *Acta Materialia* 61(15) (2013) 5743-5755.
- [6] Z. Wu, H. Bei, G.M. Pharr, E.P. George, *Acta Materialia* 81 (2014) 428-441.
- [7] A.S. Tirunilai, T. Hanemann, C. Reinhart, V. Tschan, K.P. Weiss, G. Laplanche, J. Freudenberger, M. Heilmaier, A. Kauffmann, *Materials Science and Engineering: A* 783 (2020) 139290.
- [8] G. Laplanche, A. Kostka, C. Reinhart, J. Hunfeld, G. Eggeler, E.P. George, *Acta Materialia* 128 (2017) 292-303.
- [9] J. Miao, C.E. Slone, T.M. Smith, C. Niu, H. Bei, M. Ghazisaeidi, G.M. Pharr, M.J. Mills, *Acta Materialia* 132 (2017) 35-48.
- [10] B. Gludovatz, A. Hohenwarter, K.V. Thurston, H. Bei, Z. Wu, E.P. George, R.O. Ritchie, *Nat Commun* 7 (2016) 10602.
- [11] G. Laplanche, P. Gadaud, C. Bärsch, K. Demtröder, C. Reinhart, J. Schreuer, E.P. George, *Journal of Alloys and Compounds* 746 (2018) 244-255.
- [12] N.L. Okamoto, S. Fujimoto, Y. Kambara, M. Kawamura, Z.M. Chen, H. Matsunoshita, K. Tanaka, H. Inui, E.P. George, *Scientific Reports* 6 (2016) 35863.
- [13] Z. Wu, Y. Gao, H. Bei, *Acta Materialia* 120 (2016) 108-119.
- [14] K. Lu, A. Chauhan, D. Litvinov, M. Walter, A.S. Tirunilai, J. Freudenberger, A. Kauffmann, M. Heilmaier, J. Aktaa, *Materials Science and Engineering: A* 791 (2020) 139781.

- [15] K. Liu, M. Komarasamy, B. Gwalani, S. Shukla, R.S. Mishra, *Scripta Materialia* 158 (2019) 116-120.
- [16] M.A. Hemphill, T. Yuan, G.Y. Wang, J.W. Yeh, C.W. Tsai, A. Chuang, P.K. Liaw, *Acta Materialia* 60(16) (2012) 5723-5734.
- [17] Y.-K. Kim, G.-S. Ham, H.S. Kim, K.-A. Lee, *Intermetallics* 111 (2019) 106486.
- [18] Y. Tian, S. Sun, H. Lin, Z. Zhang, *Journal of materials science & technology* 35(3) (2019) 334-340.
- [19] S.A.A. Shams, G. Jang, J.W. Won, J.W. Bae, H. Jin, H.S. Kim, C.S. Lee, *Materials Science and Engineering: A* 792 (2020) 139661.
- [20] J. Rackwitz, Q. Yu, Y. Yang, G. Laplanche, E.P. George, A.M. Minor, R.O. Ritchie, *Acta Materialia* (2020).
- [21] K.V.S. Thurston, B. Gludovatz, Q. Yu, G. Laplanche, E.P. George, R.O. Ritchie, *Journal of Alloys and Compounds* 794 (2019) 525-533.
- [22] P. Li, S. Li, Z. Wang, Z. Zhang, *Progress in Materials Science* 56(3) (2011) 328-377.
- [23] P. Lukáš, M. Klesnil, J. Krejčí, *physica status solidi (b)* 27(2) (1968) 545-558.
- [24] U. Essmann, H. Mughrabi, *Philosophical Magazine A* 40(6) (1979) 731-756.
- [25] J. Polák, V. Mazánová, M. Heczko, I. Kuběna, J. Man, *Fatigue & Fracture of Engineering Materials & Structures* 40(7) (2017) 1101-1116.
- [26] S. Lavenstein, Y. Gu, D. Madisetti, J.A. El-Awady, *Science* 370 (6513) (2020) eabb2690.
- [27] G.M. Castelluccio, D.L. McDowell, *International Journal of Plasticity* 98 (2017) 1-26.
- [28] D. Hull, D.J. Bacon, *Introduction to dislocations*, Butterworth-Heinemann 2001.
- [29] S. Suresh, *Fatigue of materials*, Cambridge university press 1998.
- [30] C.W. Shao, P. Zhang, Y.K. Zhu, Z.J. Zhang, J.C. Pang, Z.F. Zhang, *Acta Materialia* 134 (2017) 128-142.
- [31] P. Li, S.X. Li, Z.G. Wang, Z.F. Zhang, *Acta Materialia* 129 (2017) 98-111.
- [32] A.S. Tirunilai, J. Sas, K.-P. Weiss, H. Chen, D.V. Szabó, S. Schlabach, S. Haas, D. Geissler, J. Freudenberger, M. Heilmaier, A. Kauffmann, *Journal of Materials Research* 33(19) (2018) 3287-3300.
- [33] N.L. Okamoto, K. Yuge, K. Tanaka, H. Inui, E.P. George, *AIP Advances* 6(12) (2016) 125008.
- [34] C. Varvenne, A. Luque, W.A. Curtin, *Acta Materialia* 118 (2016) 164-176.
- [35] M. Schneider, E.P. George, T.J. Manescau, T. Zálezák, J. Hunfeld, A. Dlouhý, G. Eggeler, G. Laplanche, *International Journal of Plasticity* 124 (2020) 155-169.
- [36] S.S. Manson, *Behavior of materials under conditions of thermal stress*, National Advisory Committee for Aeronautics 1953.
- [37] L.F. Coffin Jr, *Transactions of the American Society of Mechanical Engineers*, New York 76 (1954) 931-950.
- [38] G.E. Dieter, D. Bacon, *Mechanical metallurgy*, McGraw-hill New York 1986.
- [39] G. Laplanche, A. Kostka, O. Horst, G. Eggeler, E.P. George, *Acta Materialia* 118 (2016) 152-163.
- [40] M.S. Pham, S.R. Holdsworth, K.G.F. Janssens, E. Mazza, *International Journal of Plasticity* 47 (2013) 143-164.
- [41] R. Zhang, S. Zhao, J. Ding, Y. Chong, T. Jia, C. Ophus, M. Asta, R.O. Ritchie, A.M. Minor, *Nature* 581 (7808) (2020) 283-287.
- [42] H. Mughrabi, *Metallurgical and Materials Transactions A* 40(6) (2009) 1257-1279.
- [43] S.N. Monteiro, H.J. Kestenbach, *Metallurgical Transactions A* 6(4) (1975) 938.
- [44] H.J. Kestenbach, *The Philosophical Magazine: A Journal of Theoretical Experimental and Applied Physics* 36(6) (1977) 1509-1515.
- [45] H. Mughrabi, *Acta Metallurgica* 31(9) (1983) 1367-1379.
- [46] J. Nellesen, S. Sandlöbes, D. Raabe, *Acta Materialia* 87 (2015) 86-99.
- [47] M.S. Pham, C. Solenthaler, K.G.F. Janssens, S.R. Holdsworth, *Materials Science and Engineering: A* 528(7-8) (2011) 3261-3269.